OPEN CHANNEL FLOW STRATIFIED BY A SURFACE HEAT FLUX

John R. Taylor
Department of Mechanical and Aerospace Engineering,
University of California, San Diego
La Jolla, CA
j2taylor@ucsd.edu

Sutanu Sarkar
Department of Mechanical and Aerospace Engineering,
University of California, San Diego
La Jolla, CA
sarkar@ucsd.edu

Vincenzo Armenio
Dipartimento di Ingegneria Civile, Universita degli Studi di Trieste,
Trieste, Italy
varmenio@units.it

ABSTRACT

Large Eddy Simulation (LES) has been used to study flow driven by a constant pressure gradient in an open channel with stable stratification imposed by a constant heat flux at the free surface and an adiabatic bottom wall. Under these conditions a turbulent mixed layer develops underneath a strongly stratified pycnocline. Turbulent properties in the pycnocline and at the free surface are examined as a function of the imposed stratification. It is found that increasing the friction Richardson number, a measure of the relative importance of stratification with respect to boundary layer turbulence, leads to a stronger, thicker pycnocline which eventually limits the impact of wall-generated turbulence on the free surface. Increasing stratification also leads to an increase in the pressure-driven mean streamwise velocity near the free surface and a corresponding increase in mean shear, a decrease in the turbulent Reynolds stress, and a substantial decrease in the eddy viscosity. PDF's and visualizations are employed to understand how stratification affects the interaction of bottom turbulence with the free surface.

MOTIVATION

The present study considers open channel flow with stable stratification imposed by a constant heat flux at the free surface and an adiabatic lower wall. This choice of boundary conditions allows us to distinguish between buoyancy effects at the turbulence generation site and in the outer region of the flow. Specifically, since the near wall region remains unstratified, the interaction between wall-generated turbulence and an external stable stratification is examined. Several previous studies have considered stratified channel flow, but in each case stratification was applied with fixed temperature boundaries. Armenio and Sarkar (2002) used a LES to study stratified closed channel flow with a fixed temperature difference ΔT across the channel. Nagaosa and Saito (1997) considered a DNS of open channel flow with fixed ΔT across the channel and a friction Reynolds number of 150. Komori et al. (1983) used steam to heat the surface of water in an inclined open channel, approximately equivalent to fixed temperature boundary conditions (Garg et al. 2000). One of the common conclusions of these studies is that for large ΔT applied across the channel, the near wall turbulent production is reduced by stratification.

Since all previous studies of stratified open channel flow have considered fixed temperature walls, the near-wall region did not remain unstratified, and hence one of the major influences of stratification was a reduction of the near-wall turbulence production. When considering environmental flows, the results of these studies may be analogous to the atmospheric surface boundary layer under conditions of strong surface cooling where a stably stratifying heat flux at the ground can lower turbulent production in the surface layer (Mahrt 1999). In contrast, our proposed boundary conditions are more relevant to the oceanic bottom boundary layer where the bounding surface is adiabatic, for example, see Lien and Sanford (2004) for a good explanation of the differences between atmospheric and oceanic boundary layers.

FORMULATION

The geometry of the open channel considered here is shown in Figure 1. Flow is driven by a uniform pressure gradient aligned with the x-axis, and periodicity is applied in both horizontal directions while flat no-slip and no-stress surfaces bound the bottom and top respectively. For simplicity, the free surface is assumed to be undeformed, a good approximation for the low Froude number flow considered here. The y-axis is aligned with the cross-stream direction, and the z-axis is

normal to the wall. Velocities in the x,y, and z directions are denoted by u,v, and w and the domain size in the x and y directions is $2\pi h$ and πh respectively, where h is the channel depth. The constant, negative density gradient imposed at the free surface can be thought of as surface heating with a constant heat flux if density changes are linearly related to temperature changes. The total density is given by $\rho_T = \rho_0 + \rho^*(\mathbf{x}, t)$, with $\rho^* << \rho_0$, allowing the Boussinesq approximation shown to be good for stratified water flows.

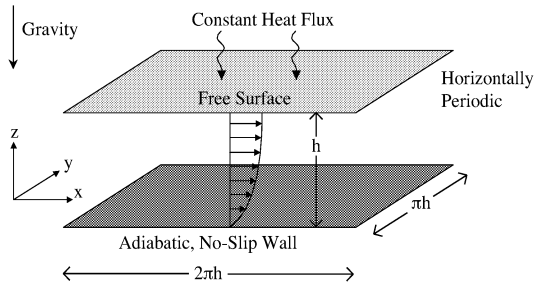

Figure 1: Model Domain

The governing equations are nondimensionalized with the channel height h, friction velocity $u_\tau = (\tau_w/\rho_0)^{\frac{1}{2}}$, and the absolute value of the imposed free surface gradient $|\partial\rho^*/\partial z|_s$. The shear stress, τ_w, used to define the friction velocity is the horizontally averaged value at the wall which must balance the vertically integrated pressure gradient for steady state, $\Pi h =< \tau_w >$. With these choices, the nondimensional governing equations can be written:

$$\frac{D\mathbf{u}}{Dt} = -\nabla p^* + \frac{\nabla^2 \mathbf{u}}{Re_\tau} - Ri_\tau \rho^* \hat{\mathbf{k}} + \Pi \hat{\mathbf{i}}, \tag{1}$$

$$\frac{D\rho^*}{Dt} = \frac{\nabla^2 \rho^*}{Re_\tau Pr}, \tag{2}$$

$$\nabla \cdot \mathbf{u} = 0, \tag{3}$$

$$z = 0: \quad u = v = w = 0, \quad \frac{d\rho^*}{dz} = 0 \tag{4}$$

$$z = 1: \quad \frac{\partial u}{\partial z} = \frac{\partial v}{\partial z} = w = 0, \quad \frac{d\rho^*}{dz} = -1, \tag{5}$$

where Π is the imposed pressure gradient equal to unity with the present nondimensionalization, and the hydrostatic pressure has been cancelled in the usual way. The nondimensional Reynolds, Richardson, and Prandtl numbers are defined as:

$$Re_\tau = \frac{u_\tau h}{\nu}, \quad Ri_\tau = -\frac{g}{\rho_0}\frac{\partial \rho^*}{\partial z}_s \frac{h^2}{u_\tau^2}, \quad Pr = \frac{\nu}{\kappa}, \tag{6}$$

where κ is the molecular diffusivity. Notice that since the imposed surface density gradient is used to make the density nondimensional, it appears in the Richardson number defined in (6); therefore increasing Ri_τ is physically equivalent to increasing the imposed surface stratification. When $Ri_\tau = 0$, density acts as a passive scalar and the velocity field can be checked against previous unstratified open channel studies. When $Ri_\tau > 0$, a negative density gradient is imposed at the free surface, corresponding to stable stratification.

Table 1: Bulk Properties

Ri_τ	Ri_b	Re_τ	Re_b	Pr
0	0	400	7132	5
25	0.04818		7150	
100	0.1927		7179	
250	0.4818		7269	
400	0.7708		7445	
500	0.9635		7539	

At statistical steady state, the nondimensional density is a linear function of time, and can be decomposed:

$$\rho^* = \rho_1(t) + \rho(\mathbf{x}, t), \tag{7}$$

where $\rho(\mathbf{x}, t)$ is the turbulent density field that is *statistically steady* and $\rho_1(t)$ denotes the deterministic field that decreases in time owing to the imposed surface heating. It can be shown that:

$$\rho_1(t) = -\frac{t}{Re_\tau Pr}. \tag{8}$$

After each time integration of (1) - (3), the density change owing to $\rho_1(t)$ is subtracted, and henceforth we will present results concerning $\rho(\mathbf{x}, t)$, the statistically steady turbulent field.

The large eddy simulation (LES) used here is the same as that used by Armenio and Sarkar (2002). A dynamic mixed subgrid model is used which has been shown to achieve proper dependence of the turbulent Prandtl number on the gradient Richardson number. The filtered equations are integrated using a version of the fractional-step method of Zang et al. (1994), which is second order accurate in space and time. A dynamic eddy diffusivity model is used for the subgrid density flux, see Armenio and Sarkar (2002) for more details.

RESULTS

Mean Profiles

We begin by describing some mean flow properties. Averages over the horizontal plane and time are denoted by $< \cdot >$. The average streamwise velocity profile, nondimensionalized by u_τ, is shown versus z/h in Figure 2(a). Note that $< u >$ and the mean shear increase in a region near the free surface where stratification is large. This is also reflected in the bulk Reynolds number, $Re_b = U_b h/\nu$, shown in Table 1 to increase with bulk Richardson number. Nagaosa and Saito (1997) also observe an increase in the streamwise velocity when they apply a fixed temperature difference across the channel to produce stable stratification. The region of increased velocity in their case extends from the surface to about 10 wall units from the lower wall, a much thicker region than is seen here. A convenient measure of the bulk change in streamwise velocity is the skin-friction coefficient:

$$C_f = 2\tau_w/\rho U_b^2. \tag{9}$$

Table 2 gives C_f for each case of Ri_τ. For comparison, the values found by Nagaosa and Saito (Nagaosa and Saito 1997) are also shown. $Ri_{\tau,\Delta}$ defined with the density difference across the channel,

$$Ri_{\tau,\Delta} = \frac{gh\Delta\rho}{\rho_0 u_\tau^2}, \tag{10}$$

is introduced to measure stratification on a similar basis in all studies. Clearly C_f decreases with $Ri_{\tau,\Delta}$ in both studies, but the dependence observed here is much weaker than the 31% decrease between $Ri_{\tau,\Delta} = 0$ and 20 observed by Nagaosa and Saito (1997). This can be explained by the relatively limited region affected by stratification in the present study, a qualitative difference with respect to the previous fixed ΔT cases.

Table 2: Skin-friction coefficient

Taylor et al., 2005			Nagaosa and Saito, 1997	
Ri_τ	$Ri_{\tau,\Delta}$	$C_f * 10^3$	$Ri_{\tau,\Delta}$	$C_f * 10^3$
0	0	6.291	0	8.71
25	0.67	6.258	10	7.06
100	3.1	6.213	20	6.03
250	12.9	6.054		
400	33	5.765		
500	51.3	5.629		

The averaged density profile for each case is plotted as a function of nondimensional height in Figure 3(a) where the density is made nondimensional by $\Delta\rho$, the difference between wall and surface values as in Komori (1983). The laminar solution to the density equation with the appropriate boundary conditions is also shown. Unlike the gradual variation of $\rho(z)$ in the laminar case, the turbulent flow exhibits a strongly stratified region, or pycnocline, near the free surface that overlies a well-mixed region near the lower wall. The presence of the well-mixed region must depend on the existence of active turbulence since the density gradient of the laminar solution vanishes only near the wall. The thickness of the pycnocline increases with Ri_τ, implying that the turbulence generated near the lower wall is less effective at mixing for large Ri_τ. Figure 3(b) shows the variation of $\Delta\rho$ between cases. $\Delta\rho$ tends to increase with increasing Ri_τ (increasing stabilization) but, even for the largest $Ri_\tau = 500$ considered here, $\Delta\rho$ is much smaller than in the laminar case.

The buoyancy or Brunt-Vaisala frequency, N defined as:

$$N^2 = \frac{-g}{\rho_0}\frac{\partial < \rho >}{\partial z}, \tag{11}$$

is shown in the left panel of figure 4. This plot makes clear the deepening and strengthening of the pycnocline with increasing Ri_τ. A local measure of the relative importance of stratification and shear, the gradient Richardson number can be defined using N and the mean shear, $S = d < u > /dz$ so that $Ri_g = N^2/S^2$, is also shown in figure 4. The gradient Richardson number measures the relative importance of turbulent production by the mean shear, and suppression by the stable stratification. As such, it is associated with

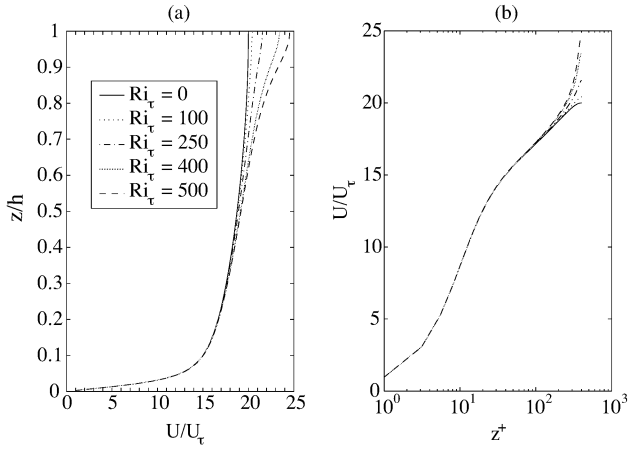

Figure 2: Mean Velocity Profile

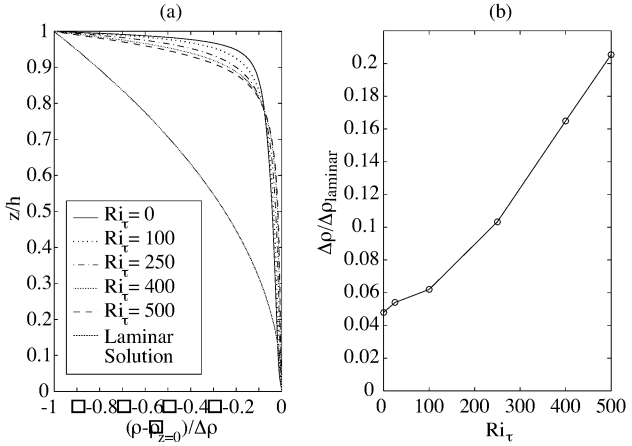

Figure 3: Mean density profiles and density difference across channel

the stability of the flow, with linear instability possible only if $Ri_g < 1/4$ somewhere in the domain. Knowing that the stratification near the surface changes significantly with Ri_τ, it is surprising that above the linear stability threshold, Ri_g is nearly independent of Ri_τ. Evidently the increase in mean shear compensates for the increase in N in this region.

TURBULENCE CHARACTERISTICS

Figure 5(a) shows the profile of the rms vertical velocity. In the lower half of the channel, the profiles collapse and are consistent with unstratified closed channel flow. In the upper region, w_{rms} decreases monotonically with increasing Ri_τ. Since w_{rms} corresponds to the vertical turbulent kinetic energy, and Ri_τ is linked to the size of the buoyancy suppression term in the TKE budget, the observed decrease is as anticipated. Interestingly, near the free surface where w_{rms} is supressed by the geometry, the dependence on Ri_τ is lost.

The Reynolds shear stress, $< u'w' >$ is shown in Figure 5(b). For comparison, the total shear stress, $\tau(z) = \tau_{wall}(1 - z/h)$ is also plotted. It can be shown (eg. Pope (2000)) that the viscous shear stress is the difference

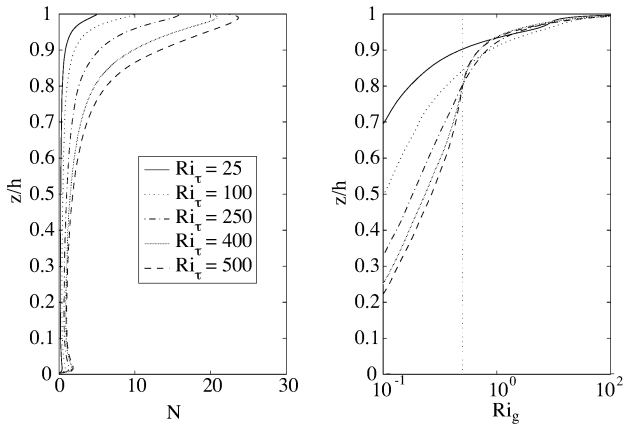

Figure 4: Brunt-Vaisala Frequency and Gradient Richardson number

between this line and $< u'w' >$. Thus, the increase in the mean vertical shear (equivalently viscous shear stress) in the pycnocline, and therefore $< u >$ at the free surface, occurs because of the stratification induced decrease in the magnitude of $< u'w' >$, which is strongest when $Ri_\tau = 500$. The drop in $< u'w' >$ magnitude will be explained using energy arguments in the section on turbulence-surface interactions.

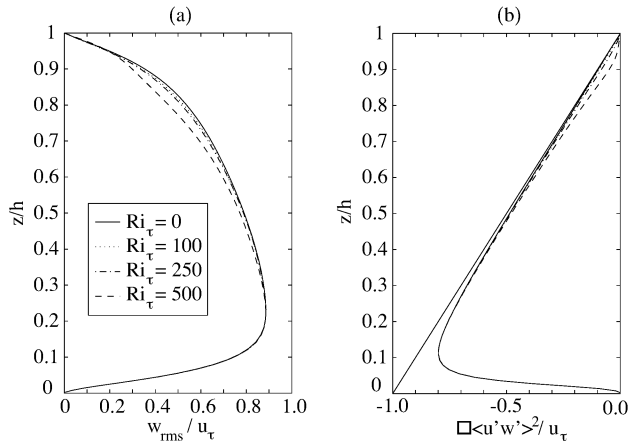

Figure 5: *rms* vertical velocity and Reynolds shear stress

Contributions to the Reynolds stress can be seen by plotting u' vs. w' as shown in Figure 6 for $z/h = 0.84$. In each quadrant of the plots is a label showing its contribution to $< u'w' > /u_\tau^2$. The upwelling events can be clearly seen for $Ri_\tau = 0$ as an anisotropic tail extending to the upper left. When $Ri_\tau = 500$ the strength of the upwellings is diminished, and the distribution becomes more isotropic. In both cases, downwelling events are not as energetic as upwelling bursts, and contribute less to $< u'w' >$.

While it has been seen that the influence of Ri_τ on C_f is rather small, the *local* turbulent diffusion is strongly affected in a significant portion of the channel, as can be seen by considering the eddy viscosity, ν_T:

$$- < u'w' > = \nu_T \frac{d < u >}{dz}. \qquad (12)$$

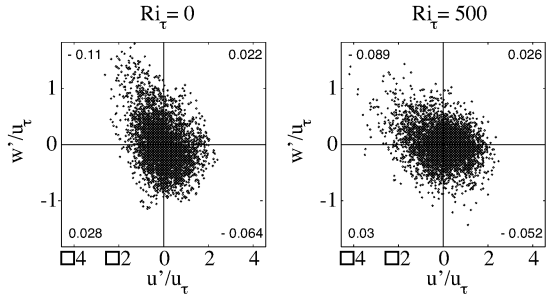

Figure 6: u' vs w' at z/h=0.84

.

The mean streamwise stress balance can then be written:

$$\tau_w(1 - \frac{z}{h}) = \frac{d < u >}{dz}(\frac{1}{Re_\tau} + \nu_T), \qquad (13)$$

so any change in the mean shear between cases must also be reflected in the eddy viscosity, plotted in Figure 7(a). Eddy viscosity decreases very significantly with Ri_τ, even in the interior of the open channel where stratification is relatively low.

Figure 7 shows the buoyancy flux, $< \rho'w' >$ nondimensionalized by the free surface density gradient, the channel height, and u_τ. Vertical motion under the negative mean density gradient implies a positive buoyancy flux for the usual case of co-gradient transport. The buoyancy flux decreases everywhere with increasing Ri_τ and has a small countergradient value near the surface when $Ri_\tau = 500$. Countergradient transport is associated with falling heavy fluid that releases potential energy to kinetic energy. Komori et al. (1983) also find a countergradient heat flux, although they report it being much larger and appearing at lower Ri_τ than in the present simulations. The difference is presumably due to the boundary conditions, since in the Komori et al. (1983) experiments, the wall and free surface were roughly held at fixed temperature. Large countergradient buoyancy fluxes were also seen in the study by Armenio and Sarkar (2002) in a closed channel with fixed temperature boundary conditions at the walls. The mass diffusivity, κ_T defined as:

$$< w'\rho' > = -\kappa_T \frac{d\rho}{dz}, \qquad (14)$$

also decreases very significantly with Ri_τ at nearly every vertical level (not shown).

TURBULENCE-SURFACE INTERACTIONS

The increase in $< u >$ seen near the free surface in the highly stratified cases can be attributed to a potential energy barrier owing to the presence of the pycnocline. It has been shown previously (Pan and Banerjee 1995) that a large portion of the Reynolds stress near an unstratified free surface in open channel flow is due to impinging of low-speed fluid advected from the near wall region. While the wall generated low speed streaks do not maintain coherence over distances comparable to the channel height in this study, low-speed ejections from the wall boundary layer are observed to directly impact the free surface in the low stratification cases.

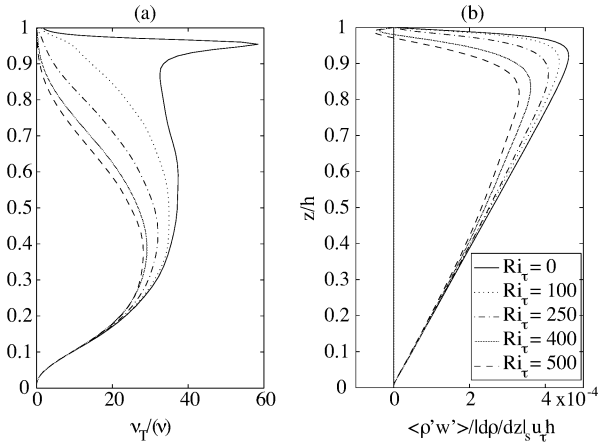

Figure 7: Eddy viscosity and buoyancy flux

That the upward advection of low speed fluid to the surface is inhibited for large Ri_τ is implied by the drop in correlation between u' and w' in the Reynolds stress of figure 5(b). To determine the fate of turbulence generated near the lower wall more directly, it is useful to consider an energy balance. Traditionally, the buoyancy scale w_{rms}/N gives a measure of how far a fluid parcel would travel vertically if all of its vertical turbulent kinetic energy were converted to potential energy. For the situation considered here, this is not accurate since N is highly variable in the vertical direction. For instance, in the highly active region near the lower wall, w_{rms} is large while N is small, so the buoyancy scale may be very large. However, the presence of a strong pycnocline near the surface adds to the potential energy barrier, and may prevent direct interaction with the surface.

As a more accurate measure of the ability of local turbulence to reach the free surface, we compare the vertical turbulent kinetic energy (TKE) to the potential energy deficit relative to the free surface. This ratio, plotted in the left panel of figure 8 is:

$$\frac{g\int_z^h (<\rho>(z) - <\rho>(z'))dz'}{\frac{1}{2}<w'w'>}. \qquad (15)$$

As expected, this ratio is largest when $Ri_\tau = 500$ since this case has a stronger, deeper pycnocline, requiring more energy to reach the free surface. The cases with the lowest stratification, namely $Ri_\tau = 25$ and $Ri_\tau = 100$, have small values of this ratio. That the pycnocline is weak in relation to the vertical TKE helps to explain why these cases are quite similar to the passive scalar case, $Ri_\tau = 0$. The case of $Ri_\tau = 250$ appears to be 'transitional' since the energy ratio is about one at most locations. Meanwhile, the strength of the pycnocline dominates over the vertical TKE when $Ri_\tau = 500$. Since the low-speed fluid near the wall, on the average, does not have sufficient energy to reach the surface in the latter case, a drop in $< u'w' >$ is observed near the surface and, correspondingly, there is an increase in $< u >$. It should be noted that since this ratio is an *average* measure, it does not preclude the instantaneous advection of bottom fluid to the surface, but does indicate that it is much less likely when a strong pycnocline exists.

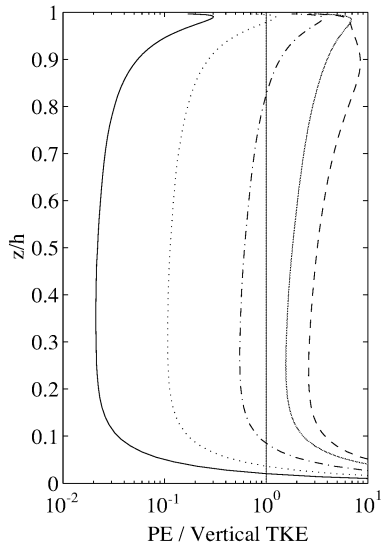

Figure 8: Ratio of potential energy deficit to vertical TKE

The strength and frequency of upwelling events can be quantified with a joint probability density function (PDF) of the vertical velocity, w, and density anomaly, $\rho'(\mathbf{x},t) = \rho(\mathbf{x},t) - <\rho>(z)$ as shown in Figure 9 for $Ri_\tau = 0$ and 500 at $z/h = 0.975$. The figure caption lists the values of ρ' corresponding to the mean density at the top and bottom for comparison. The plot indicates that when $Ri_\tau = 500$, it is very rare for fluid with density equal to the mean at $z = 0$ (corresponding to $\rho' = 0.077$ and well out of the plotted region) to be seen at this height. For the case of $Ri_\tau = 0$ it is common to see $\rho' = 0.008$, the mean at $z = 0$, and the free surface value $\rho' = -0.014$ is somewhat less likely. The tails of the w distribution are wider when $Ri_\tau = 0$ and $\rho' > 0$; a large w and $\rho' > 0.008$ is associated with the strong upwelling events seen when $Ri_\tau = 0$ and mentioned previously. For the case of $Ri_\tau = 0$ large w events of both signs are associated with positive density anomaly and the distribution is nearly symmetric about $w = 0$. Evidently, at this location, the downwellings of dense fluid are as strong and frequent as the upwellings. When $Ri_\tau = 500$, the largest vertical velocities are no more likely to be associated preferentially with either heavy or light fluid, indicating that events with upwelling of dense fluid are not dominant. The off-centered maxima of the ρ' distributions are presumably due to the asymmetry in ρ' associated with the top and bottom of the channel for each case.

The effect of stratification on dense fluid upwellings near the free surface can also be clearly seen by examining the instantaneous property distributions. Figure 10 shows ρ' and w', the deviation from the horizontal mean, at $z/h = 0.999$ for $Ri_\tau = 0$ and $Ri_\tau = 500$ at the last simulation time in both cases. The height of the surface mesh denotes the vertical velocity with the tall peaks indicating rising fluid ($w' > 0$). The corresponding grayscale shows ρ' with dark gray denoting heavy fluid with positive ρ'. Notice that for $Ri_\tau = 0$, each region of upwelling is associated with a positive density anomaly indicating an upwelling of dense fluid from the bottom. When $Ri_\tau = 500$ none of the positive w' patches at this particular time are associated

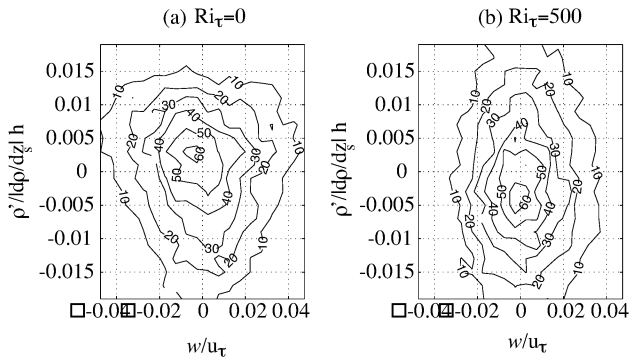

Figure 9: Joint PDF between vertical velocity, w and density anomaly, $\rho'(\mathbf{x},t) = \rho(\mathbf{x},t) - <\rho>(z)$ at z/h=0.975 for (a) $Ri_\tau = 0$, (b) $Ri_\tau = 500$. The density anomalies corresponding to $<\rho>$ at the top and bottom respectively are -0.014 and 0.008 for $Ri_\tau = 0$, and -0.026 and 0.077 for $Ri_\tau = 500$.

with large positive ρ'. These snapshots are typical of those seen throughout the simulation; while the existence of dense fluid upwellings cannot be precluded for the strongest stratification cases, they are much less common than when $Ri_\tau = 0$.

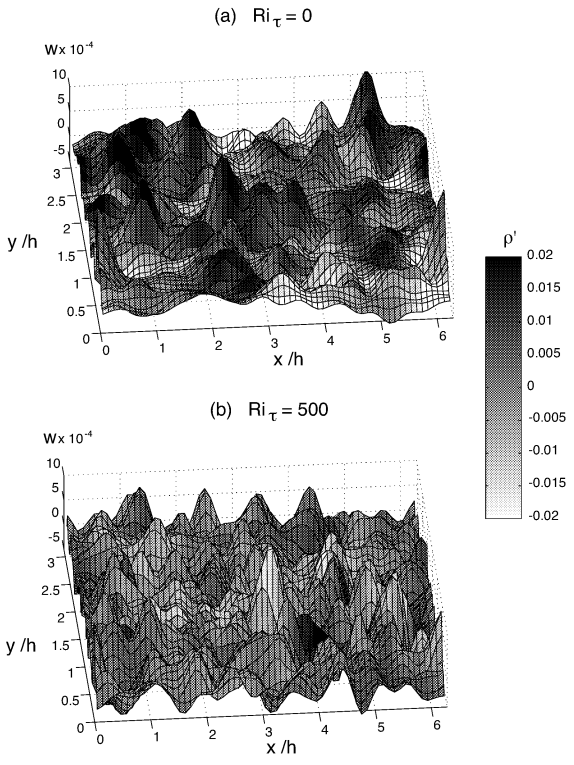

Figure 10: Instantaneous height maps of vertical velocity with density perturbation in grayscale

CONCLUSION

Turbulent open channel flow with an imposed density gradient at the free surface corresponding to surface heating and an adiabatic bottom boundary is studied here and the effects of changing the friction Richardson number, Ri_τ, are examined. In all cases, a stably stratified pycnocline overlies a lower region that is well mixed by turbulence generated at the lower wall. As Ri_τ is increased, the turbulence in the mixed region remains unchanged while the turbulence in the pycnocline is affected by buoyancy, but never completely suppressed. It is possible that by sufficiently increasing Ri_τ, the flow in the pycnocline could relaminarize, although this limit is not obtained here. It is observed that increasing Ri_τ results in an increase in the bulk Reynolds number, Re_b, and a deepening and strengthening of the pycnocline. The mean velocity deviates from the log law with the extent of the deviation systematically increasing with Ri_τ. Since the gradient Richardson number is too large in the pycnocline for local turbulent production, the influence of increasing Ri_τ can be explained by a potential energy barrier affecting the interaction of bottom boundary layer turbulence with the surface region. Visualizations and joint PDFs of ρ' and w show that upwelling of dense bottom fluid to the surface becomes rare in the large Ri_τ cases.

*

References

Armenio, V. and S. Sarkar (2002). An investigation of stably-stratified turbulent channel flow using large eddy simulation. *J. Fluid Mech. 459*, 1–42.

Garg, R., J. Ferziger, S. Monismith, and J. Koseff (2000). Stably stratified turbulent channel flows. I. Stratification regimes and turbulence suppression mechanism. *Phys. Fluids A 12*, 2569–2594.

Komori, S., H. Ueda, F. Ogino, and T. Mizushina (1983). Turbulence structures in stably stratified open-channel flow. *J. Fluid Mech. 130*, 13–26.

Lien, R. and T. Sanford (2004). Turbulence spectra and local similarity scaling in a strongly stratified oceanic bottom boundary layer. *Continental Shelf Research 24*, 375–392.

Mahrt, L. (1999). Stratified atmospheric boundary layers. *Boundary-Layer Meteorology 90*, 375–396.

Nagaosa, R. and T. Saito (1997). Turbulence structure and scalar transfer in stably stratified free-surface flows. *AIChE J. 43*, 2393.

Pan, Y. and S. Banerjee (1995). A numerical study of free-surface turbulence in channel flow. *Phys. Fluids 7*, 1649–1664.

Pope, S. (2000). *Turbulent Flows*. Cambridge: Cambridge University Press.

Zang, Y., R. Street, and R. Koseff (1994). A non-staggered grid, fractional step method for time-dependent incompressible Navier-Stokes equations in curvilinear coordinates. *J. Comput. Physics 114*, 18–33.